DOCKING ALIGNMENT-3D-QSAR OF A NEW CLASS OF POTENT AND NON-CHIRAL INDOLE-3-CARBOXAMIDE-BASED RENIN INHIBITORS

Jahan B. GHASEMI[1,*] and Somayeh PIRHADI[2]

Chemistry Department, Faculty of Sciences, K. N. Toosi University of Technology, Tehran, Iran; e-mail: [1] jahan.ghasemi@gmail.com, [2] so.pirhadi@gmail.com

Received April 9, 2011
Accepted July 12, 2011
Published online December 4, 2011

Using generated conformations from docking analysis by CDOCKER algorithm, some 3D-QSAR models; CoMFA region focusing (CoMFA-RF) and CoMSIA have been created on a series of a new class of potent and non-chiral renin inhibitors. The satisfactory predictions were obtained by CoMFA-RF and CoMSIA based on docking alignment in comparison to CoMFA. Robustness and predictability of the models were further verified by using the test set, cross validation (leave one out and leave ten out), bootstrapping, and progressive scrambling. All-orientation search (AOS) strategy was used to acquire the best orientation and minimize the effect of the initial orientation of aligned compounds. The results of 3D-QSAR models are in agreement with docking results. Moreover, the resulting 3D CoMFA-RF/CoMSIA contour maps and corresponding models were applied to design new and more active inhibitors.

Keywords: Enzymes; Drug design, Drug discovery; CoMFA; CoMSIA; CDOCKER; Realignment; Renin inhibitors.

Hypertension is a main risk feature of high occurrence worldwide for cardiovascular diseases[1]. Different signals, for instance a drop in blood pressure, a decrease in the plasma sodium, or a reduction in the circulating volume, stimulate the release of renin from kidney[2]. Renin is an aspartic acid protease in the beginning of renin angiotensin system (RAS) cascade, one of the key regulators of blood pressure. The only known natural substrate for renin is angiotensinogen, and renin cleaves it to form a decapeptide, angiotensin I. Then angiotensin converting enzyme (ACE) catalyses conversion of angiotensin I to an octapeptide vasoconstrictor angiotensin II, which has a direct action on proximal tubule, to increase reabsorbing sodium and moreover motivate adrenal cortex to sprinkle aldostrone, that in turn acts upon the distal nephron to retain sodium leading to fluid retention[3]. ACE inhibitors, increase the level of angiotensin I, and do not block manufacture of angiotensin II, that are independent from ACE. Also ACE is

doi:10.1135/cccc2011070

not a specific enzyme, as a result has some side effects, such as persistent dry cough[4]. On the other hand renin has a known substrate and renin inhibitors not only have superior blood pressure reducing effects but also exhibit optimal end organ conservation that inhibition of renin would be an attractive solution for the control of hypertension[5]. Early renin inhibitors were peptidic and suffered from poor pharmacokinetic properties and were synthetically challenging[6]. Aliskiren as a highly efficient, nonpeptidic renin inhibitor was discovered by Ciba-Geigy after rigorous research for many years[7–9]. But nowadays some research groups endeavor to synthesize simpler and more bioavailable renin inhibitors[10,11].

Traditional QSAR models consider neither the 3D structures of compounds nor their chirality and are not sufficient to state complex structure-activity relationships, because the extreme specificity of biological activity is explained by three dimensional (3D) intramolecular forces[12–18]. On the other hand, classical QSAR equation do not directly propose new compounds to synthesize[19]. Comparative molecular field analysis (CoMFA)[20] belongs to a series of powerful computational methods in rational design of novel inhibitors and related applications. In this method, steric and electrostatic fields surrounding a set of aligned molecules in a grid box are sampled and correlated with observed activities. In a similar method, comparative molecular similarity indices analysis (CoMSIA), a probe atom is used to calculate similarity indices, at regularly spaced grid points for the aligned molecules. CoMSIA differs from CoMFA, initially in the way that the molecular fields are calculated. CoMSIA uses Gaussian-based similarity functions for molecular field calculations, while CoMFA predominantly uses force field like potentials (e.g., Lennard-Jones and Coulomb)[20–23]. In computational drug design, docking tools apply to gain key structural features of binding of an inhibitor into the receptor and predicting bioactive conformers.

In this study, 3D-QSAR approaches based on docking conformers were applied to construct predictive 3D-QSAR models on a new class of non-chiral indole-3-carboxamide-based renin inhibitors. The obtained quantitative models were applied to design new and more potent inhibitors.

EXPERIMENTAL

Dataset

A collection of 40 compounds were reported recently by B. Scheiper and co-workers[24], as a new class of potent and non-chiral indole-3-carboxamide-based renin inhibitors, were used for docking and 3D-QSAR analysis. IC_{50} (μM) values were taken in molar range and were ex-

pressed in negative logarithmic units, pIC_{50} (–log IC_{50}), in order to give consistent numerical values. The set of inhibitors was divided into training and test sets. The test set compounds were selected by considering both the distribution of biological data and structural diversity of the molecules. Structures and IC_{50} values of training and test set compounds are shown in Tables Ia–Ic. At first 33 of inhibitors were used as the training set and 7 for the test set, then two compounds (**22** and **23**) showing large residual values, were identified as outliers and removed from the training set.

Molecular Docking

The crystal structures of three inhibitors **1**, **13** and **36**, forming complexes with human renin, are 3OQK, 3OQF and 3OOT, respectively. These structures were taken from RCSB protein databank (http://www.pdb.org). In ligand preparation step, structures of other compounds were constructed via modifying these compounds in SYBYL 7.3 molecular modeling package (Tripos Inc., St. Louis, USA) running on a Red Hat Linux workstation 4.7. The resulting structures were transferred into Discovery Studio 2.5 (Accelrys Inc, San Diego, CA, USA) and typed with CHARMm force field, and partial charges were calculated by Momany–Rone option[25]. The resulting structures were minimized with Smart Minimizer which performs 1000 steps of steepest descent with a RMS gradient tolerance of 3, followed by Conjugate Gradient minimization[26]. For preparation step of enzymes, all complexes were typed with CHARMm force field, hydrogen atoms were added, all water molecules were removed, and pH of protein was adjusted to almost neutral, 7.4, using protein preparation protocol. All inhibitors were again minimized in situ with Smart Minimizer option that is custom for in situ Ligand Minimization and consists of some pre-defined minimization steps that have been pre-determined to work well for receptor ligand data[26]. A 7.5 Å radius sphere was defined around the bounded ligands to confirm atoms of each ligand, and the side-chains of the residues of the receptor within 7.5 Å from the centre of the binding site are free to move. Then bounded inhibitors were removed from the binding site. Other parameters were established by default protocol settings. CDOCKER (CHRMm-based DOCKER) and a molecular dynamics (MD) simulated-annealing based algorithm were used to dock inhibitors into the receptors. CDOCKER is an implementation of a CHARMm based docking tool using a rigid receptor that generates several prime random ligand orientations within the receptor active site followed by MD-based simulated annealing, and final refinement by minimization. During the docking, van der Waals (vdW) and electrostatics (non-bonded interactions) are softened at different levels, but this softening is deleted for the ultimate minimization[27]. This molecular docking technique needs a site sphere around the ligand that radius was set to 7.5 Å in this approach. For each final conformation, the CDOCKER score was accounted as the negative value (interaction energy plus ligand strain) and employed to rank the poses of every input ligand[27].

CoMFA and CoMSIA

The best pose of each inhibitor was selected and docked conformers were fed to SYBYL molecular modeling package. All current charges were removed and partial atomic charges were calculated using the Gasteiger–Hückel method. The correctness of the prediction of CoMFA and CoMSIA models are strongly dependent on the structural alignment of the compounds. Two strategies were employed to construct 3D-QSAR models. In first approach, docked bioactive conformers were aligned inside the active site of protein (Fig. 1a) and in a hybrid

TABLE Ia
In vitro renin activity (IC_{50}) for compounds **1–15**

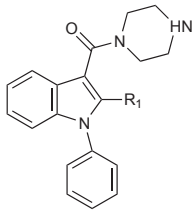

Compound No.	R_1	Renin IC_{50}, μM
1[a]	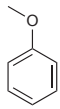	0.420
2	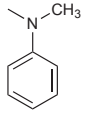	3.160
3	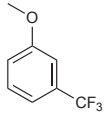	9.000
4	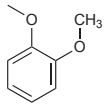	0.680
5	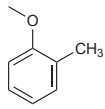	0.021
6	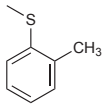	0.071
7	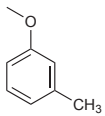	0.773

TABLE Ia
(*Continued*)

Compound No.	R_1	Renin IC_{50}, μM
8	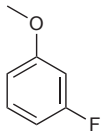	0.063
9[a]	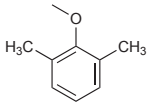	0.064
10	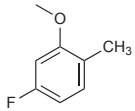	0.005
11	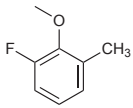	0.016
12	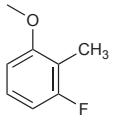	0.011
13	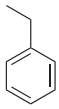	0.091
14	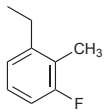	0.009
15	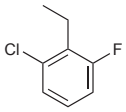	0.018

[a] Prediction set.

TABLE Ib
In vitro activity for compounds **16–25**

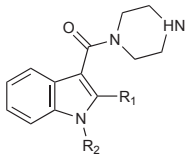

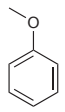

R_1 = A

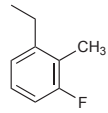

R_1 = B

Compound No.	R_1	R_2	Renin IC_{50}, μM
16[a]	A	2-pyridyl	4.970
17	A	4-fluorophenyl	0.709
18	A	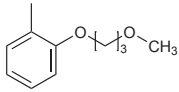	0.175
19	A	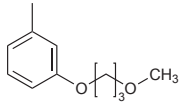	0.763
20	B	cyclohexyl	0.034
21[a]	B	cyclopentyl	0.020
22	B	4-pyranyl	0.752
23	B	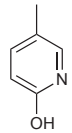	9.350
24	B	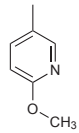	0.360
25	B	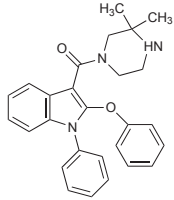	7.3

[a] Prediction set.

strategy all conformers from docking were realigned to the template molecule (compound **36** in this case) on a common backbone with minimizing the sum-of-squares deviation between reference backbone in each inhibitor and the corresponding core in the template, to put all conformations into a common Cartesian coordinate syste (Fig. 1b). Since CoMFA models are greatly sensitive to the different space orientations of the molecular collective with respect to the grid box, all-orientation search (AOS) was also carried out on initial orientations of aligned structures by the rotation procedure written in SYBYL programming language (SPL)[28]. In CoMFA a probe sp^3 carbon atom with +1 charge was employed, and steric and electrostatic interactions between the probe and structures were calculated. Electrostatic interactions were modeled using a Coulomb potential, and van der Waals interac-

TABLE Ic
In vitro activity for compounds **26–40**

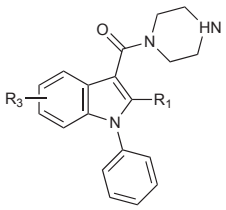

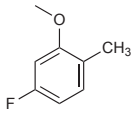

R_1 = A

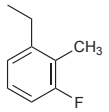

R_1 = B

Compound No.	R_1	R_3	Renin IC_{50}, μM
26[a]	A	6-OCH_3	0.024
27	A	5-OCH_3	1.350
28	A	5-OH	0.002
29	A	5-$CONH_2$	0.006
30	A	6-COOH	0.122
31	A	6-$OCH_2CH_2N(CH_3)_2$	0.029
32	A	6-OCH_2COOH	0.130
33	B	6-OCH_3	0.012
34	B	6-OH	0.004
35[a]	B	5-OH	0.004
36	B	4-CH_3, 5-OH	0.002
37	B	7-F	0.084
38	B	6-OCH_2CH_2OPh	0.024
39	B	6-OCH_2CH_2OH	0.031
40	B	5-SO_2CH_3	0.044

[a] Prediction set.

tion using a Lennard-Jones potential. Various column filtering values are also tested. CoMFA standard scaling applies the equal weight to data from each lattice point in any given field. Region focusing is an iterative procedure which refines a model by improving the weight for those lattice points which are most related to the model. This enhances the resolution and predictive capability (q^2; cross validated r^2) of a followed PLS analysis. Technically, this corresponds to rotate the model components during a high-order space[29]. PLS region focusing is rationally equivalent to the GOLPE strategy and q^2-GRS [30,31]. T32he standard settings (probe with charge +1, radius 1 Å and hydrophobicity +1, hydrogen-bond donating +1, hydrogen-bond accepting +1, attenuation factor α of 0.3, and grid spacing 2 Å) were used in CoMSIA to compute five different fields, viz. steric, electrostatic, hydrophobic, acceptor and donor. PLS analysis was used for the 3D-QSAR in which the independent variables were the CoMFA and CoMSIA fields, and pIC_{50} data values were used as dependent variables.

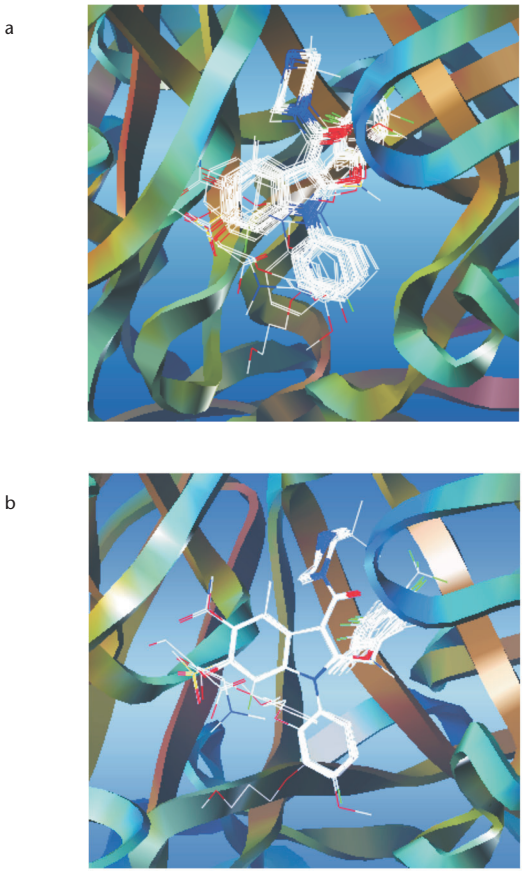

FIG. 1
Alignment of compounds based on (a) docking alignment inside the active site and (b) generated conformations from docking and then rigid body alignment based on compound **36**

RESULTS AND DISCUSSION

Docking Study

Docking computations were employed to find the probable binding conformations of all renin inhibitors. To validate the docking reliability, root-mean-square distance (RMSD) value was calculated between bounded inhibitors and redocked ligands, which for compounds **1**, **13** and **36** were 0.63, 0.36 and 0.29, respectively. These values show a high reliability of CDOCKER method to reproduce the known binding mode of these inhibitors. The crystallographic structure with the best resolution, 3OOT, was used in subsequent docking and molecular modeling. Comparison of CDOCKER scores (from 0.38894 to –15.0097) of docked ligands show, all active compounds ($pIC_{50} > 8$) have the CDOCKER score more negative than –12.5. The compound **23** (the least active compound in the set) has the unusual high score (–15.65) which shows it was not correctly docked.

CoMFA and CoMSIA Studies

PLS analysis of the docking alignment of the compounds in the training set expressed a CoMFA-region focusing (CoMFA-RF) QSAR model (grid spacing = 1) with a good q^2 value of 0.649 (six components) that is superior to CoMFA. The outlier status of compound **22** in all 3D-QSAR models indicates its structural strangeness as it is a sole compound which bears a pyranyl substituent among all dataset. Also since compound **23** cannot be correctly docked, its orientation is not as other compounds in the set, and was regarded as outlier. The optimal number of components was determined by selecting the highest q^2 value corresponds to lowest S_{press} value. The non-cross-validated PLS analysis results in a high conventional r^2 = 0.985, F = 257.121, a low standard error of estimation (SEE) of 0.139, with a column filtering of 2.0. The contributions of steric and electrostatic fields were 0.539 and 0.461, respectively. Figure 2a shows the relationship between the experimental and predicted pIC_{50}.

The CoMSIA analysis was done at a grid spacing 2 Å, and the effect of column filtering was checked with the combination of five fields. The CoMSIA method defines explicit hydrophobic and hydrogen bond donor and acceptor descriptors in addition to the steric and electrostatic fields in CoMFA. To select the optimal results, we systematically changed the combination of fields, and hydrophobic and electrostatic fields have cleared contribution on the improving internal predictivity of models. By assuming the combi-

nation of five fields, q^2 of 0.542 was obtained with five components at a column filtering of 2.5 kcal/mol, F = 164.239, non-cross-validated r^2 = 0.970, and SEE = 0.189. The corresponding field contributions of steric, electrostatic, hydrophobic, hydrogen bond donor and hydrogen bond acceptor are 0.128, 0.340, 0.224, 0.173 and 0.135, respectively. The more contribution of electrostatic and hydrophobic fields shows the more impor-

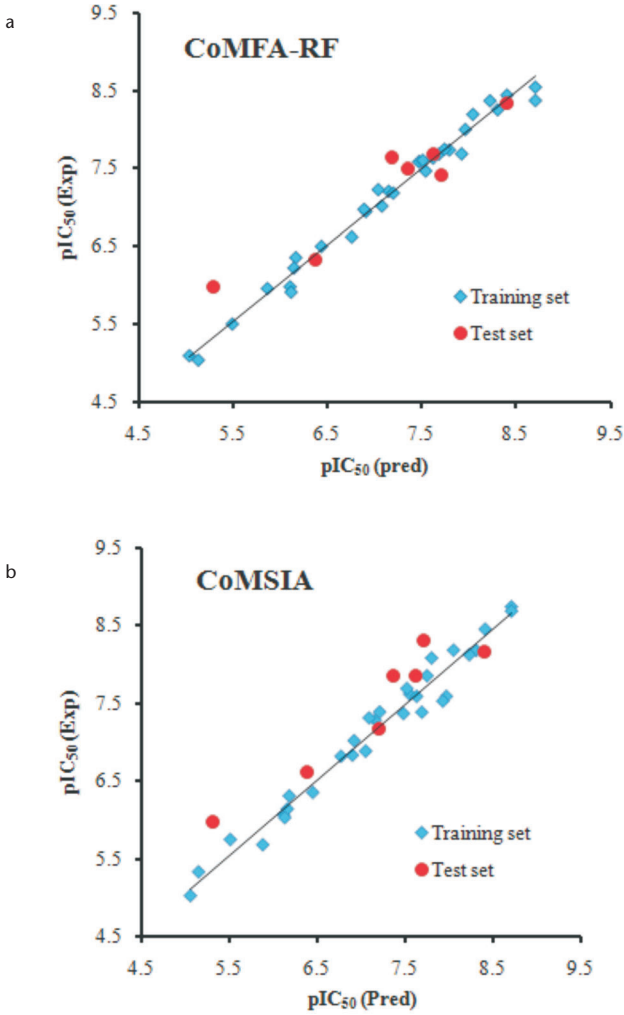

FIG. 2
Observed against predicted activities for the training and test sets of compounds by docking alignment based on CoMFA-RF (a) and CoMSIA (b) models

TABLE II
The experimental pIC_{50} values, predicted pIC_{50} values and the residuals of the training and test set compounds based on docking alignment

Compound No.	Experimental	CoMFA-RF		CoMSIA	
		Pred.	Res.	Pred.	Res.
1[a]	6.38	6.32	0.06	6.61	–0.23
2	5.5	5.50	0.00	5.74	–0.24
3	5.05	5.09	–0.04	5.02	0.03
4	6.17	6.36	–0.19	6.30	–0.13
5	7.68	7.69	–0.01	7.38	0.30
6	7.15	7.21	–0.07	7.28	–0.13
7	6.11	5.98	0.13	6.06	0.05
8	7.2	7.19	0.01	7.38	–0.18
9[a]	7.19	7.64	–0.45	7.17	0.02
10	8.3	8.26	0.04	8.18	0.12
11	7.79	7.74	0.05	8.08	–0.29
12	7.96	8.00	–0.04	7.59	0.37
13	7.04	7.23	–0.19	6.88	0.16
14	8.04	8.20	–0.16	8.18	–0.14
15	7.74	7.75	–0.01	7.85	–0.11
16[a]	5.3	5.99	–0.69	5.98	–0.68
17	6.15	6.22	–0.07	6.14	0.01
18	6.76	6.62	0.14	6.82	–0.06
19	6.12	5.91	0.21	6.02	0.10
20	7.47	7.59	–0.12	7.36	0.11
21[a]	7.7	7.41	0.29	8.31	–0.61
24	6.44	6.50	–0.06	6.35	0.09
25	5.14	5.04	0.10	5.33	–0.19
26[a]	7.62	7.69	–0.07	7.85	–0.23
27	5.87	5.96	–0.09	5.68	0.19

TABLE II
(*Continued*)

Compound No.	Experimental	CoMFA-RF		CoMSIA	
		Pred.	Res.	Pred.	Res.
28	8.7	8.55	0.15	8.74	–0.04
29	8.22	8.38	–0.16	8.12	0.10
30	6.91	6.95	–0.04	7.02	–0.11
31	7.54	7.47	0.07	7.62	–0.08
32	6.89	6.98	–0.09	6.83	0.06
33	7.92	7.69	0.23	7.52	0.40
34	8.4	8.45	–0.05	8.45	–0.05
35[a]	8.4	8.34	0.06	8.16	0.24
36	8.7	8.13	0.57	8.68	0.02
37	7.08	7.02	0.06	7.31	–0.23
38	7.62	7.64	–0.02	7.59	0.03
39	7.51	7.61	–0.10	7.69	–0.18
40[a]	7.36	7.49	–0.13	7.86	–0.50

[a] Prediction set.

tance of these fields to enhance activity. The correlation between the experimental and predicted activities is depicted in Fig. 2b. The experimental and predicted activities for training and test set compounds with CoMFA-RF and CoMSIA models are shown in Table II.

In addition to the 3D-QSAR studies using the docking alignment described above, all conformers from docking realigned to the template molecule (compound **36** in this case). Since all conformers of docking process were used, and compounds of **22** and **23** were docked differently from the rest of the compounds, they were again outliers from the beginning. A CoMFA-RF 3D-QSAR model with a q^2 value of 0.534 with 3 PLS components was obtained. Similarly, CoMSIA 3D-QSAR study was conducted on the compounds in the realignment method. CoMSIA PLS analysis afforded a modest q^2 value of 0.412 with 3 PLS components. The statistical results of both alignment strategies are shown in Table III.

TABLE III
Summary of the statistical results for the constructed models

Statistical Parameters[a]	Docking alignment[b]		Realignment	
	CoMFA-RF (CF = 2.0)	CoMSIA (CF = 2.5)	CoMFA-RF (CF = 2.5)	CoMSIA (CF = 3.0)
q^2	0.649	0.542	0.534	0.412
SEP	0.665	0.744	0.722	0.811
r^2_{ncv}	0.985	0.970	0.798	0.801
SEE	0.139	0.189	0.476	0.472
F_{ratio}	257.121	164.239	35.481	36.167
r^2_{pred}	0.911	0.896	0.626	0.614
Component	6	5	3	3

[a] Statistical parameters have their original meanings. [b]The superior alignment method. CF – column filtering

Validation of the 3D-QSAR Models Based on Docking Alignment

The external set of 7 compounds were used to confirm predictive ability of the models. The r^2_{pred} from docking based CoMFA-RF and CoMSIA models was found to be 0.911 and 0.896, respectively, which show models that have acceptable predictability. To evaluate the statistical confidence limits of the derived models, bootstrapping[20] analysis was carried out with 100 runs. Bootstrapping involves the generation of many new datasets from the original dataset after randomly choosing samples from that. A r^2_{bs} (average correlation coefficient for bootstrapping) of 0.993 ± 0.004 and a SEE_{bs} (average standard error of estimate for bootstrapping) of 0.089 ± 0.065 for CoMFA-RF model, and r^2_{bs} of 0.978 ± 0.011 and a SEE_{bs} of 0.155 ± 0.104 for CoMSIA model, suggested a good internal consistency and the absence of systematic errors of the models. To evaluate the sensitivity of the optimized CoMFA-RF and CoMSIA models to chance correlations, the leave-one-out (LOO), leave 10-out cross-validation and progressive scrambling analyses were performed[32]. q^2 of leave 10-out for CoMFA-RF and CoMSIA models, were 0.637 and 0.514, respectively. In the progressive scrambling approach, small random perturbations are introduced into a data set and the statistical results, the perturbation prediction (q^2), the calculated cross-validated standard error of prediction (cSDEP) as the function of the correlation coef-

ficient between the true values (y) of the dependent variables and the perturbed values (y') of the dependent variables, and the slope of q^2 (cross validated correlation coefficient) with respect correlation of the original dependent variables against the perturbed dependent variables ($dq^{2'}/dr^2_{yy'}$), for CoMFA-RF and CoMSIA models are summarized in Table IV.

TABLE IV
Model progressive scrambling for CoMFA-RF and CoMSIA models based on docking alignment

Model	q^2	cSDEP	$dq^{2'}/dr^2_{yy'}$
CoMFA-RF	0.485	0.811	1.052
CoMSIA	0.421	0.825	0.740

CoMFA, CoMSIA, and Docking Interpretation

The renin protein binding site has a 'closed-flap' conformation[33]. Renin S_3 and S_1 subsites construct a large hydrophobic cavity and the formation of van der Waals get in touch with to the hydrophobic amino acids lining the S_3-S_1 cavity are energetically favorable for binding affinity[34]. The hydrophobic side chains lining the margins of S_3 and S_1 are Thr12, Gln13, Pro111, Phe112, Leu114, Ala115, Phe117, Ser219 and Val30, Asp32, Tyr75, Thr77, Phe112, Phe117, Val120, Asp215 [35]. Also a discrete narrow channel buried in native renin, that is extended from the S_3 site perpendicular to the active site cleft toward the center of the enzyme present[35–37] that, now in general termed S_3sp (S_3 subpocket), occupied by ordered water molecules and is not involved in substrate or peptide-based inhibitor binding[34]. S_3sp is a potential auxiliary binding site. Key side chains lining the boundaries of S_3sp are Thr12, Gln13, Tyr14, Val30, Tyr155, Thr216, Gly217, Ser219 and Ala303 [34]. Figure 3 shows amino acids constructing S_1, S_3 and S_3sp. Optimization of the mostly hydrophobic interactions inside the S_3sp, noticeably improved binding affinity for renin, and selectivity in comparison to related aspartic peptidases[37]. But the corresponding vector for the indole scaffold is a little deviating from the narrow entrance into this subpocket, which might explain the less pronounced effect of this substitution compared to other series like Aliskiren analogs[24,38,39].

CoMSIA steric, electrostatic, hydrophobic, hydrogen bond donor and acceptor field contour maps are shown in Figs 4a–4e, respectively. The contours of the steric map are shown in yellow and green, and those of the

electrostatic map are shown in red and blue. Greater values of 'Bio-Activity Measurement' are correlated with: more bulk near green, less bulk near yellow, more positive charge near blue, and more negative charge near red. The yellow and white contours in hydrophobic fields depict hydrophobic and hydrophilic favored regions, and the acceptor field contains information about where hydrogen bond donating groups should be on the receptor. The acceptor field contour shows regions where hydrogen bond donors on the receptor are predicted to enhance (magenta) and disfavor (red) binding, respectively, and the donor favored field (cyan) where acceptors on the receptor are predicted to favor binding and disfavored donor field (purple) where acceptor on the receptor is predicted to disfavor binding. Looking at the contours in the renin binding pocket shows that the sterically favorable green contour lies within the S_1 pocket, while the sterically unfavorable contours intersect the MOLCAD surface, that it reinforces the validity of the model. A yellow contour is around ortho-substitution of R_1, indicates that a less bulky group would be favorable and a green contour near ortho-substitution of R_1 explains a more bulky the group increases activity, it shows that why activity of compounds **5**, **6**, **9–12**, and **14**, **15** with methyl or F substituents instead H at R_1 ortho-substitution is higher than compound **1**, and compound **5** (R_1 ortho-methyl, IC_{50} = 0.021) is more active than **9** (R_1 ortho- and ortho'-methyl, IC_{50} = 0.064). The R_1 ortho-substitutions are in van der Waals interactions with hydrophobic parts of Val30, Gly217 and Phe117, and optimally fill the hydrophobic subsite of S_1. On the other

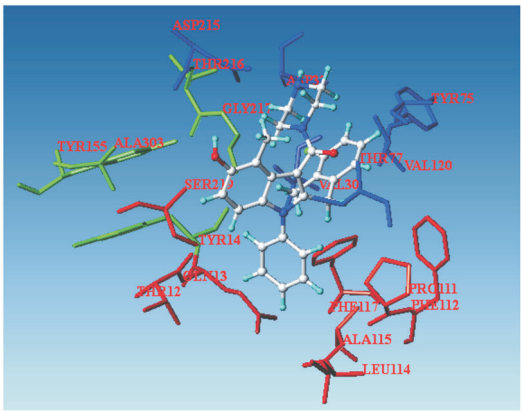

FIG. 3
Amino acids which construct S_1 (blue), S_3 (red) and S_3sp (green) renin binding sites. Common residues colored in same color

hand, ortho'-F position of R_1 is in van der Waals contacts with aromatic ring of Tyr75, Phe112, and polar NH and OH of Thr77. But more bulky groups such as methyl because of probable steric clashes with boundaries of S_1 pocket would decrease the activity in contrast of ortho'-F substituent: activity of compound **11** (ortho' = –F, IC_{50} = 0.016) > **9** (ortho' = $–CH_3$, IC_{50} = 0.064), also **14** (IC_{50} = 0.009) > **15** (ortho'-Cl, IC_{50} = 0.018). Activity of com-

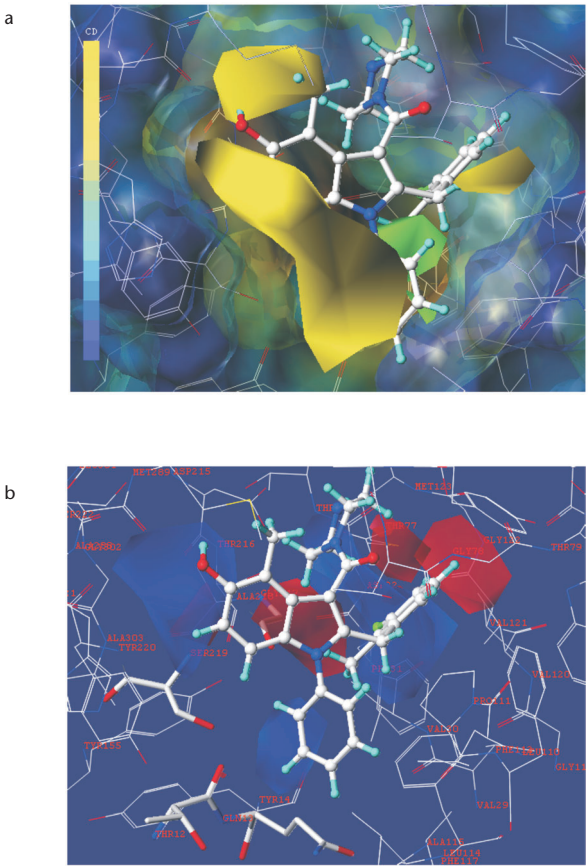

FIG. 4

Std* coeff CoMSIA contour maps displaying steric, electrostatic, hydrophobic, hydrogen bond donor and acceptor features based on compound **36**. a Steric contour maps. The MOLCAD multi-channel surfaces structure depicted with cavity depth potential of the renin pocket using compound **36**. The cavity depth color ramp ranges from blue (low depth values – outside of the pocket) to light red (high depth values – cavities deep inside the pocket). b Electrostatic contour maps. c Hydrophobic contour maps. d Hydrogen bond donor contour maps. e Hydrogen bond acceptor contour maps

c

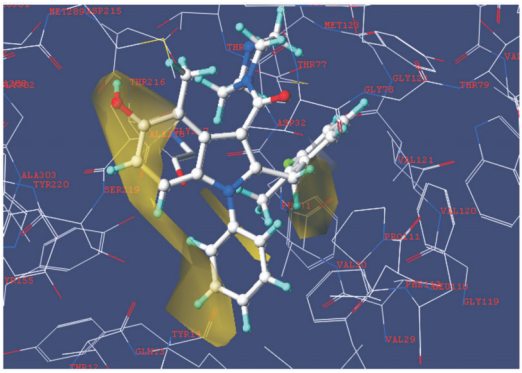

d

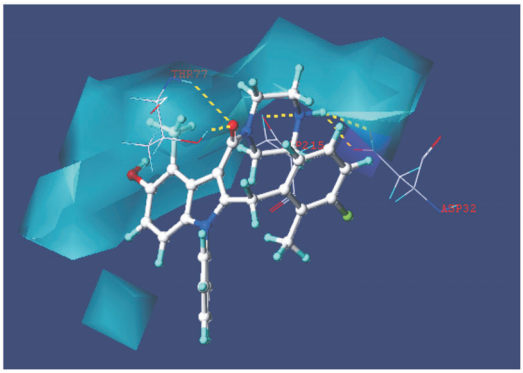

e

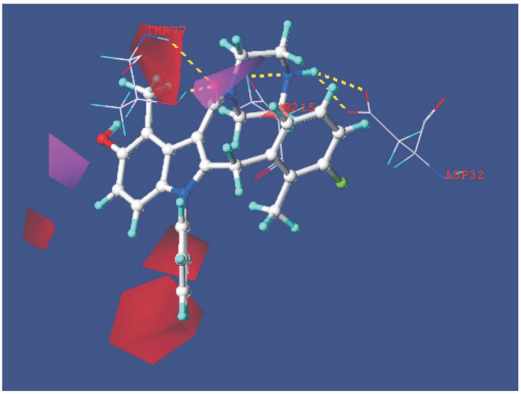

FIG. 4
(*Continued*)

pound **2** is less than compound **1**, since the yellow contour is near N-CH_3 in R_1, then it may smash with S_3 or S_1 walls. The large regions of yellow contours near the 4–7th substitutions of indole core indicating that less bulky groups would be favored. It is caused by the models the proximity of 4th and 5th groups to Ser76, Thr77, Ala218, Ser219, Met289, and 6th and 7th substitutions to Gly217, Ala218, Ser219, and Tyr220 and probable steric clashes with them. This can be explained by the order of the activities: **5** (IC_{50} = 0.021) > **26** (R_3 = 6-OMe, IC_{50} = 0.024). Compounds **38** and **31** are more active than compound **39**, because in **38** (6-OCH_2CH_2OPh, IC_{50} = 0.024) and **31** (6-$OCH_2CH_2N(CH_3)_2$, IC_{50} = 0.029) R_3 is oriented out of the binding site whereas R_3 substituent in **39** (6-OCH_2CH_2OH, IC_{50}= 0.031) is inside the active site and near the S_3 wall cavity. As a result for R_3 substitutions inside the cavity, less bulky groups are favored. The electrostatic contour maps based on compound **36**, are shown in Fig. 4b. The red contours on meta- and meta′-position of R_1, explain more electronegative groups are favored in such a way that meta- and meta′-F in both phenoxy and benzyl increased the inhibitory activity: **8** (meta-F, IC_{50} = 0.063) > **1** (meta-H, IC_{50} = 0.420). Also compounds **12** (meta-F, IC_{50} = 0.011), and **10** (meta′-F, IC_{50} = 0.005) > **5** (meta- and meta′-H, IC_{50} = 0.021). It can be on near contact of meta′-F with aromatic ring of Tyr75, and interaction of meta-F with Val30 and carbon atoms of Asp32 [24]. This red contour confirms activity of compound **7** (meta-CH_3, IC_{50} = 0.773) is lower than compound **8** (meta-F, IC_{50} = 0.063). The blue, and cyan contours near 5-position of indole core reveals the positive charge increases inhibitory activity, it can be on the electrostatic interaction of 5-OH with NH of Ala288. It can explain why presence of 5-OH is favored and the most active compounds in the set (**36** and **28**) have OH in 5-position. The presence of both electrostatic blue and red contours near indole 6-position pointed out that the electrostatic effect at this region is not very important for inhibitory activity. For example, activity of compound **30** with a more electron-withdrawing group (6-CO_2H, IC_{50} = 0.122) is lower than that of compound **26** with a more electron-donating group (6-OCH_3, pIC_{50} = 0.024). On the other hand compound **34** (6-OH, IC_{50} = 0.004) is more active than compound **33** (6-OCH_3, IC_{50} = 0.012). There is a blue contour beside substitutions of N_1-phenyl ring of indole (R_2), explain more electropositive groups increase the activity. It is due to adjacency of these positions to the polar residues: Thr12, Gln13, and Ser219. Also presence of disfavored red contour of hydrogen bond acceptor shows these substitutions should be more electropositive. It can explain why activity of compound **1** (R_2 = phenyl, IC_{50} = 0.420) is more than com-

pound **16** (R_2 = 2-pyridyl, IC_{50} = 4.970). A red electrostatic contour and a magenta hydrogen bond acceptor favored cover carboxamide oxygen, which shows presence of the electronegative and hydrogen bond acceptor, carbonyl group, beside OH of Thr77, in this region is favored. The blue contour coat O or C-linker in phenoxy or benzyl substitutions indicates this order of activity: **13** (R_1 = benzyl, IC_{50} = 0.091) > **1** (R_1 = phenoxy, IC_{50} = 0.420), and **14** (IC_{50} = 0.009) > **12** (IC_{50} = 0.011), also O-linker is electron-withdrawing whereas O in Gly217 is electronegative and prefers to interact with a more electropositive group. Also it can be on the electrostatic repulsion of lone pair of O in phenoxy with lone pair of carboxamide oxygen[24]. In hydrophobic contour maps, the yellow regions are near 4–7th positions of indole core, indicating hydrophobic groups are favored to increase activity, due to the hydrophobic nature of neighbor side chains in S_3, in such a way that in addition to steric effects, activity of compound **38** (6-OCH_2CH_2OPh, IC_{50} = 0.024) is higher than compounds **39** (6-OCH_2CH_2OH, IC_{50} = 0.031), and **40** (6-SO_2CH_3, IC_{50} = 0.044). Moreover yellow hydrophobic contours are beside R_1 substitutions confirm favored interactions of hydrophobic substitutions with hydrophobic side chains of S_1 and S_3. As such a higher activity of compound **12** (R_1 ortho-CH_3, IC_{50} = 0.011) in contrast with compound **8** (R_1 ortho-H, IC_{50} = 0.063), also compound **5** (R_1 ortho-CH_3, IC_{50} = 0.021) is higher than compound **1** (R_1 = phenoxy, IC_{50} = 0.420), that are in accordance with interpretation of steric contour maps. Also yellow hydrophobic regions covered substitutions of N_1-phenyl ring, explain hydrophobic substitutions are favored to increase activity, in such a way that replacement of N_1-cyclohexyl (in compound **20**) and cyclopentyl (in compound **21**) instead N_1-phenyl (in compound **14**) could not considerably decrease activity. Based on hydrogen bond donor and acceptor fields in Figs 4d and 4e, there is a cyan contour near N of piperazine ring, indicates importance of hydrogen bond donating feature in increasing binding affinity. Also presence of electrostatic blue contour at this position confirm the cyan contour, because H atom of the NH at this position has the positive charge because of its hydrogen bonding nature. Complementary of this cyan contour in the receptor, are aspartate residues of renin Asp32 and Asp215, and this clears that any new renin inhibitor should interact with one of them[9,38,39]. There are cyan and magenta fields beside 5th and 6th position of indole core, suggest presence of hydrogen bond acceptor and donor groups in this region increase binding affinity. It can explain why activities of compounds **28** (5-OH, IC_{50} = 0.002), **29** (5-$CONH_2$, IC_{50} = 0.006), **34** (6-OH, IC_{50} = 0.004), **35** (5-OH, IC_{50} = 0.004),

and **36** (5-OH, IC_{50} = 0.002) are pretty high. There is a red acceptor contour around substituents in N_1-phenyl ring, suggest hydrogen bond acceptor groups in this region is disfavored.

Steric and electrostatic contour maps of CoMFA-RF models based on docking and realignment methods are shown in Figs 5a and 5b. The regions of the models are nearly similar to CoMSIA contour maps.

a

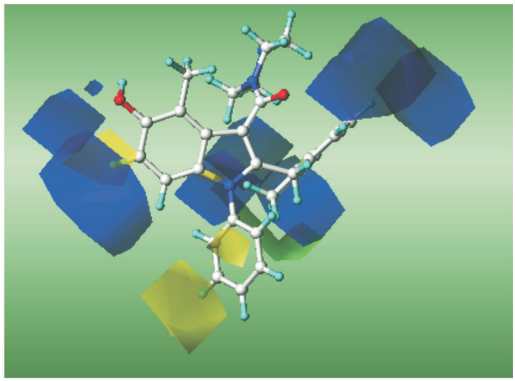

b

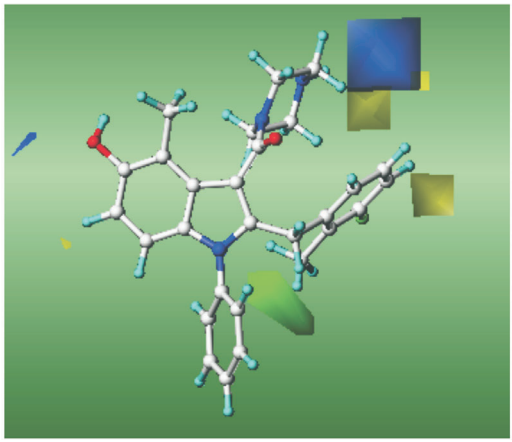

FIG. 5
Std* coeff contour maps of CoMFA models in combination with compound **36**, green contours indicate regions where bulky groups increase activity, while yellow contours indicate regions where bulky groups decrease activity. a Steric and electrostatic fields of CoMFA-RF based on docking and b realignment methods

Pharmacophore Model

A qualitative pharmacophore model was constructed to extract the common essential features among the highly active compounds using 8 compounds having activity > 8.0 (pIC_{50}) by Hip-Hop module of Discovery Studio 2.5 package. This model contains five features: three hydrophobic aromatic, one hydrogen bond acceptor, and one hydrogen bond donor. The pharmacophore model which was mapped to the highest active compound **36** was shown in the Fig. 6. The three hydrophobic aromatic features are mapped to the phenyl rings positioned at R_1, R_2 (N_1-phenyl ring), and indole core of common scaffold. The position of hydrophobic aromatic features shows the importance of hydrophobic interactions in the renin inhibitors. One hydrogen bond acceptor was mapped to the electron rich oxygen of carboxamide group beside OH of Thr77, same as were shown by magenta hydrogen bond acceptor favored and red electrostatic contours in CoMSIA model. One hydrogen bond donor feature was mapped to the NH of piperazine ring which complementary of this feature in the receptor, are hydrogen bond acceptor groups (Asp32 and Asp215). The generated pharmacophore model shows the goodness of common scaffold in this class of non-chiral renin inhibitors.

In this study, molecular docking and 3D-QSAR studies were performed on a series of newly synthesized non-chiral renin inhibitors. Docked ligands

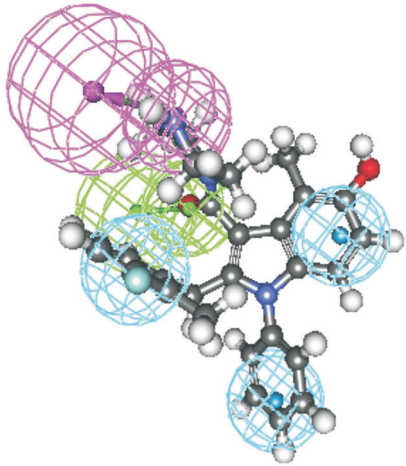

FIG. 6
Mapping of common featured pharmacophore model onto the compound **36**

were used as the bioactive conformations in subsequent 3D-QSAR studies. The CoMFA and CoMSIA analyses provided identifying key structural features influencing inhibitory activity of these inhibitors. We found and confirmed the key residues that involved in the hydrogen bond donors and hydrogen bond acceptors in addition to the hydrophobic, steric and electrostatic interactions. According to the results of this study, we successfully designed some new inhibitors with excellent predicted activities in the best CoMFA-RF and CoMSIA models. The excellent statistical parameters and the suitable predictive ability of the resulted models explain that these models can help to rational design of novel renin inhibitors with preferred activities.

REFERENCES

1. Rosamond W., Flegal K., Furie K., Go A., Greenlund K., Haase N., Hailpern S. M., Ho M., Howard V., Kissela B., Kittner S., Lloyd-Jones D., McDermott M., Meigs J., Moy C., Nic G., O'Donnell C., Roger V., Sorlie P., Steinberger J., Thom T., Wilson M., Hong Y.: *Circulation* **2008**, *117*, 25.
2. Hackenthal E., Paul M., Ganten D., Taugner R.: *Physiol. Rev.* **1990**, *70*, 1067.
3. Brewster U. C., Perazella M. A.: *Am. J. Med.* **2004**, *116*, 263.
4. Cugno M., Nussberger J., Cicardi M., Agostoni A.: *Int. J. Immunopharmacol.* **2003**, *3*, 311.
5. Ravid D., Lishner M., Lang R., Ravid M. J.: *Clin. Pharmacol.* **1994**, *3*, 1116.
6. Gradman A. H., Schmieder R. E., Lins R. L., Chiang Y., Bedigian M. P.: *Circulation* **2005**, *111*, 1012.
7. Göschke R., Stutz S., Heinzelmann W., Maibaum J.: *Helv. Chim. Acta* **2003**, *86*, 2848.
8. Wood J. M., Maibaum J., Rahuel J., Grütter M. G., Cohen N.-C., Rasetti V., Rüger H., Göschke R., Stutz S., Fuhrer W., Schilling W., Rigollier P., Yamaguchi Y., Cumin F., Baum H.-P., Schnell C. R., Herold P., Mah R., Jensen C., O'Brien E., Stanton A., Bedigian M. P.: *Biochem. Biophys. Res. Commun.* **2003**, *308*, 698.
9. Rahuel J., Rasett V., Maibaum J., Rüeger H., Göschke R., Cohen N.-C., Stutz S., Cumin F., Fuhrer W., Wood J. M., Grütter M. G.: *J. Chem. Biol.* **2000**, *7*, 493.
10. Sarver R. W., Peevers J., Cody W. L., Ciske F. L., Dyer J., Emerson S. D., Hagadorn J. C., Holsworth D. D., Jalaie M., Kaufman M., Mastronardi M., McConnell P., Powell N. A., Quin III J., Van Huis C. A., Zhang E., Mochalkin I.: *Anal. Biochem.* **2007**, *360*, 30.
11. Powell N. A., Ciske F. L., Cai C., Holsworth D. D., Mennen K., Huis C. A. V., Jalaie M., Day J., Mastronardi M., McConnell P., Mochalkin I., Zhang E., Ryan M. J., Bryant J., Collard W., Ferreira S., Gu C., Collins R., Rational J., Noel J. E.: *Bioorg. Med. Chem.* **2007**, *15*, 5912.
12. Garg R., Gupta S. P., Gao H., Babu M. S., Debnath A. K., Hansch C.: *Chem. Rev.* **1999**, *99*, 3525.
13. Concu R., Podda G., Ubeira F. M., González-Díaz H.: *Curr. Pharm. Des.* **2010**, *16*, 2710.
14. González-Díaz H., Romaris F., Duardo-Sanchez A., Pérez-Montoto L. G., Prado-Prado F., Patlewicz G., Ubeira F. M.: *Curr. Pharm. Des.* **2010**, *16*, 2737.
15. González-Díaz H., Duardo-Sanchez A., Ubeira F. M., Prado-Prado F., Pérez-Montoto L. G., Concu R., Podda G., Shen B.: *Curr. Drug Metab.* **2010**, *11*, 379.

16. González-Díaz H., Prado-Prado F., Ubeira F. M.: *Curr. Top. Med. Chem.* **2008**, *8*, 1676.
17. González-Díaz H., González-Díaz Y., Santana L., Ubeira F. M., Uriarte E.: *Proteomics* **2008**, *8*, 750.
18. González-Díaz H., Vilar S., Santana L., Uriarte E.: *Curr. Top. Med. Chem.* **2007**, *7*, 1015.
19. Verma J., Khedkar V. M., Coutinho E. C.: *Curr. Top. Med. Chem.* **2010**, *10*, 95.
20. Cramer R. D., Patterson D. E., Bunce J. D.: *J. Am. Chem. Soc.* **1988**, *110*, 5959.
21. Klebe G., Abraham U., Mietzner T.: *J. Med. Chem.* **1994**, *37*, 4130.
22. Pirhadi S., Ghasemi J. B.: *Eur. J. Med. Chem.* **2010**, *45*, 4897.
23. Ghasemi J. B., Pirhadi S., Ayati M.: *Bull. Korean Chem. Soc.* **2011**, *32*, 645.
24. Scheiper B., Matter H., Steinhagen H., Stilz U., Böcskei Z., Fleury V., McCort G.: *Bioorg. Med. Chem. Lett.* **2010**, *20*, 6268.
25. Momany F. A., Rone R. J.: *J. Comput. Chem.* **1992**, *13*, 888.
26. *Discovery Studio*. Accelrys Software Inc, San Diego (CA) 2009.
27. Guosheng W. U., Robertson D. H., Brooks III C. L., Vieth M.: *J. Comput. Chem.* **2003**, *24*, 1549.
28. Wang R. X., Gao Y., Liu L., Lai L. H.: *J. Mol. Model.* **1998**, *4*, 276.
29. *QSARTM Manual, SYBYL,* version 7.3. Tripos, St. Louis (MO) 2006.
30. Baroni M., Costantino G., Cruciani G., Riganelli D., Valigi R., Clementi S.: *Quant. Struct.–Act. Relat.* **1993**, *12*, 9.
31. Cho S., Tropsha A.: *J. Med. Chem.* **1995**, *38*, 1060.
32. Clark R. D., Fox P. C.: *J. Comput. Aided Mol. Des.* **2004**, *18*, 563.
33. Rahuel J., Priestle J. P., Grütter M. G.: *J. Struct. Biol.* **1991**, *107*, 227.
34. Webb R. L., Schiering N., Sedrani R., Maibaum J.: *J. Med. Chem.* **2010**, *53*, 7490.
35. Maibaum J., Feldman D. L.: *Annu. Rev. Med. Chem.* **2009**, *44*, 105.
36. Hanson G. J., Clare M., Summers N. L., Lim L. W., Neidhart D. J., Shieh H. S., Stevens A. M.: *Bioorg. Med. Chem.* **1994**, *2*, 909.
37. Tong L., Pav S., Lamarre D., Pilote L., LaPlante S., Anderson P. C., Jung G.: *J. Mol. Biol.* **1995**, *250*, 211.
38. Politi A., Durdagi S., Moutevelis-Minakakis P., Kokotos G., Papadopoulos M. G., Mavromoustakos T.: *Eur. J. Med. Chem.* **2009**, *44*, 3703.
39. Politi A., Durdagi S., Moutevelis-Minakakis P., Kokotos G., Mavromoustakos T.: *J. Mol. Graph. Model.* **2010**, *29*, 425.